PHYSICAL REVIEW B **87**, 161121(R) (2013)

Li_2RhO_3: A spin-glassy relativistic Mott insulator

Yongkang Luo,[1] Chao Cao,[2] Bingqi Si,[1] Yuke Li,[2] Jinke Bao,[1] Hanjie Guo,[1] Xiaojun Yang,[1] Chenyi Shen,[1] Chunmu Feng,[1] Jianhui Dai,[2] Guanghan Cao,[1] and Zhu-an Xu[1,*]

[1]*Department of Physics and State Key Laboratory of Silicon Materials, Zhejiang University, Hangzhou 310027, China*

[2]*Department of Physics, Hangzhou Normal University, Hangzhou 310036, China*

(Received 3 February 2013; revised manuscript received 4 March 2013; published 29 April 2013)

Motivated by the rich interplay among electronic correlation, spin-orbit coupling (SOC), crystal-field splitting, and geometric frustrations in the honeycomblike lattice, we systematically investigated the electronic and magnetic properties of Li_2RhO_3. The material is semiconducting with a narrow band gap of $\Delta \sim 78$ meV, and its temperature dependence of resistivity conforms to a three-dimensional variable range hopping mechanism. No long-range magnetic ordering was found down to 0.5 K, due to the geometric frustrations. Instead, single atomic spin-glass behavior below the spin-freezing temperature (~6 K) was observed and its spin dynamics obeys the universal critical slowing down scaling law. A first-principles calculation suggested it to be a relativistic Mott insulator mediated by both electronic correlation and SOC. With moderate strength of electronic correlation and SOC, our results shed light on the research of the Heisenberg-Kitaev model in realistic materials.

DOI: 10.1103/PhysRevB.87.161121 PACS number(s): 71.20.Be, 75.40.Cx, 75.10.Jm

Ternary transition metal oxides set up a fascinating platform for investigating correlated electronic systems. Depending on the particular transition metal element and crystalline structure, features such as high-temperature superconductivity (SC) in the doped spin-1/2 antiferromagnetic (AFM) Mott insulator La_2CuO_4,[1] giant negative magnetoresistance in $La_{2/3}Ba_{1/3}MnO_3$ films,[2] odd parity SC in Sr_2RuO_4,[3,4] SC in water intercalated $Na_xCoO_2 \cdot yH_2O$,[5] and field induced metamagnetic transition and quantum criticality in $Sr_3Ru_2O_7$ (Ref. 6) have been observed. Electronic correlation is expected to be strongest in 3*d* transition metals, represented by a small *d* orbital radius and a large Coulomb repulsion *U*. It weakens as one goes from 3*d* to 4*d* and 5*d* transition metals due to the spatial extension of *d* orbits. However, relativistic spin-orbit coupling (SOC) which increases with atomic number follows the opposite trend. The recently discovered exotic nonmetal behaviors in those heavy transition metal oxides[7–10] remind us of the importance of SOC in these materials. One representative example is Sr_2IrO_4,[10] which was confirmed to be a novel Mott insulator mediated by strong SOC even though the electronic correlation is relatively weak, while its structural analog Sr_2RhO_4 (Ref. 11) shows normal Fermi-liquid metallicity.

The general formula Li_2MO_3 (M = transition metal) actually describes two types of crystalline structures: Li_2MnO_3 type ($C2/m$, No. 12)[12] and Li_2SnO_3 type ($C2/c$, No. 15).[13] In both crystalline structures, the layers of MO_6 octahedral interstices are alternately filled either with Li^+ only, or with 1/3 Li^+ and 2/3 M^{4+}, as depicted in Fig. 1(a), whereas the MO_6 octahedra with M in the center form edge-sharing honeycomblike networks[14] [Fig. 1(b)]. A tiny difference between these two crystalline structures resides in the stacking of Li-M layers along the c axis: In the case of Li_2SnO_3 type, the Sn^{4+} hexagonal networks in adjacent layers are displaced by $(0,\pm 1/6,1/2)$ in lattice coordinates, while in Li_2MnO_3 type, they are displaced by $(0,1/2,1/2)$.[15] The formation of a honeycomblike MO_6 octahedral network makes Li_2MO_3 a suitable candidate for investigating the interplay among electronic correlation, SOC, crystal-field splitting, and geometric frustrations.

Li_2RhO_3 and Li_2IrO_3 crystallize in Li_2MnO_3- and Li_2SnO_3-type structures, respectively. Previously, they were studied for potential applications as Li-ion battery cathode materials.[14,16,17] More underlying physical properties still need to be explored. Herein, we systematically studied the electronic and magnetic properties of Li_2RhO_3. Our results point out that Li_2RhO_3 is likely to be a spin-glassy Mott insulator with a narrow thermal activating gap $\Delta \sim 78$ meV, while the spin-freezing temperature is sample dependent, ranging from 5 to 7 K. No long-range magnetic ordering can be captured in this frustrated system down to 0.5 K. Our experimental results were understood by first-principles calculations, which confirm the important roles played by both electronic correlation and SOC. The calculation also pointed out that Li_2RhO_3 is on the boundary of an antiferromagnetically-ferromagnetically correlated ground state, which might interpret the spin-glassy behavior observed experimentally.

A polycrystalline sample of Li_2RhO_3 was grown by the solid state reaction method as mentioned elsewhere.[14] The sample quality of Li_2RhO_3 was checked by x-ray diffraction (XRD), performed on a PANalytical x-ray diffractometer (Empyrean Series 2) with Cu$K\alpha_1$ radiation at room temperature. Lattice parameters were derived by Rietveld refinement on the RIETAN-RF program.[18] The electrical resistivity and specific heat were measured on a Quantum Design physical property measurement system (PPMS-9). The dc magnetization measurement was carried out on a Quantum Design magnetic property measurement system (MPMS-5) employing both zero-field-cooling (ZFC) and field-cooling (FC) protocols. The ac magnetic susceptibility was measured on PPMS-9 with various frequencies ranging from 10 Hz to 10 kHz.

The XRD pattern (not shown) guarantees high purity of the samples, and all the peaks can be well indexed based on the $C2/m$ (No. 12) space group which is isostructural to Li_2MnO_3. The Rietveld refinement yields $a = 5.1212(3)$ Å, $b = 8.8469(4)$ Å, $c = 5.1015(3)$ Å, $\alpha = \gamma = 90°$, and $\beta = 109.641(3)°$, which are comparable to those in the previous literature.[14] Detailed structural parameters are summarized in Table I. The labels S1 and S2 represent the two Li_2RhO_3

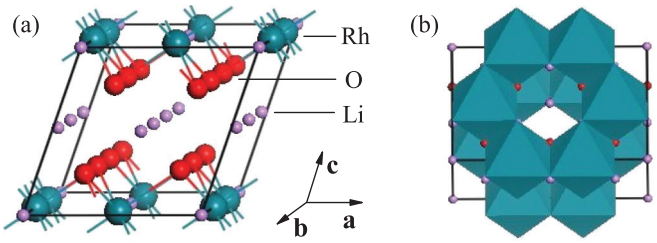

FIG. 1. (Color online) (a) The crystalline structure of Li_2RhO_3, which is stacked by alternating Li and $LiRh_2O_6$ layers. (b) Within the $LiRh_2O_6$ layer, the RhO_6 octahedra form a honeycomblike lattice.

samples annealed at 950 and 900 °C, respectively. It should be pointed out that there is an antisite disorder between Li^+ ions and Rh^{4+} ions. Such antisite disorder is a common feature in Li_2MO_3 materials,[15,16] and may have a double-sided influence on the magnetism: On the one hand, the partial substitution of M^{4+} by nonmagnetic Li^+ ions breaks the long-range magnetic coupling among M^{4+} moments, while on the other hand, it also reduces the geometric frustrations on the M^{4+} honeycomb lattice and thus stabilizes the magnetic structure.

The electrical resistivity of S1 is shown in Fig. 2, from which an insulating ρ vs T dependence is clearly seen. At 300 K, the magnitude of resistivity is 0.48 Ω cm, about two orders smaller than that of Na_2IrO_3.[9] In the inset of Fig. 2, we show the ρ vs $1/T$ in the semilogarithmic plot, and we found that the $\rho(T)$ curve does not follow well the Arrhenius law for thermally activated hopping, viz., $\rho(T) \propto \exp(\Delta/T)$, but is better fit to $\rho(T) \propto \exp[(D/T)^{1/4}]$, which is known as the three-dimensional variable range hopping (3D-VRH)[19] stemming from the random potential scattering contributed by large numbers of defects or disorders. A similar phenomenon was also observed in Na_2IrO_3,[9] and we attributed this to the defect or antisite disorder of Li and Rh, as is mentioned in Table I. A rough estimate of activating energy $\Delta \sim 78$ meV will be derived from the data 200–300 K. The measurement on S2 leads to a similar result. According to a previous work performed by Todorova *et al.*,[14] the $\rho(T)$ curve obeys the Arrhenius law for the temperature region 300–500 K, and the derived energy gap is $\Delta = 80$ meV. This magnitude of Δ is close to our result, and is much smaller than that of Na_2IrO_3 (340 meV).[20] All these confirm that Li_2RhO_3 is a narrow gap insulator.

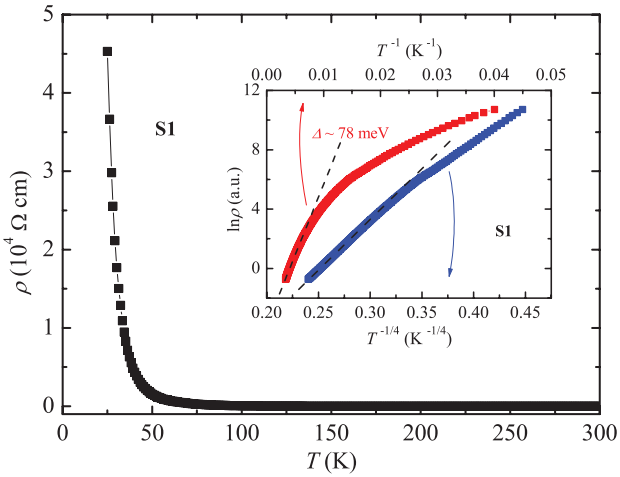

FIG. 2. (Color online) Electrical resistivity of Li_2RhO_3. The inset shows resistivity in the Arrhenius plot and 3D-VRH plot. The dashed lines are guides to eyes. The thermal activating gap $\Delta \sim 78$ meV is estimated in the Arrhenius plot.

The main frame of Fig. 3(a) displays the temperature dependence of the dc magnetic susceptibility of S1. For temperatures above 50 K, $\chi(T)$ obeys Curie-Weiss's law [see the inset of Fig. 3(a)], and can be well fitted to $\chi(T) = C/(T - \theta_W)$, where θ_W is the Weiss temperature. The fitting leads to $\theta_W = -50$ K. The negative θ_W indicates a dominant AFM coupling between Rh^{4+} moments. The fitting also derives the effective moment $\mu_{\text{eff}} = 2.03\mu_B$ (μ_B is Bohr's magnon). This magnitude of μ_{eff} is close to but relatively larger than the ideal value for a low-spin state of Rh^{4+} ($1.73\mu_B$) in the case of $J = S = 1/2$ and Landé factor $g = 2$, manifesting incompletely the quenched orbital contribution. For the low-temperature region, a sharp peak centered at 5.6 K is clearly seen in the curve for $\mu_0 H = 0.01$ T. We also observed a discrepancy between the ZFC and FC modes below this peak temperature. With increasing magnetic field, this peak loses sharpness and becomes rounded, and meanwhile the discrepancy between ZFC and FC shrinks. This field dependent $\chi(T)$ was confirmed by the isothermal magnetization measurement shown in the inset of Fig. 3(b). A tiny hysteresis loop with a remanent magnetization $1.4 \times 10^{-3}\mu_B$/Rh and a coercive field 0.6 kOe is evident at 2 K. It should be pointed out that these observations were reproducible in different batches of the

TABLE I. Rietveld refinement of Li_2RhO_3. Calculation based on space group $C2/m$ (No. 12). The derived $a = 5.1212(3)$ Å, $b = 8.8469(4)$ Å, $c = 5.1015(3)$ Å, $\alpha = \gamma = 90°$, $\beta = 109.641(3)°$. The quality factors of this refinement are $R_{wp} = 15.40\%$, $R_p = 11.89\%$, and $S = 1.79$ for S1, and $R_{wp} = 14.60\%$, $R_p = 11.05\%$, and $S = 1.71$ for S2.

Atom	Site	x	y	z	Occ.-S1	Occ.-S2
Li(1)	4*g*	0	0.333	0	0.185(5)	0.139(6)
Li(2)	2*a*	0	0	0	0.704(7)	0.721(5)
Li(3)	4*h*	0	0.833	0.5	1	1
Li(4)	2*d*	0	0.5	0.5	1	1
Rh(1)	4*g*	0	0.333	0	0.815(5)	0.861(6)
Rh(2)	2*a*	0	0	0	0.296(7)	0.279(5)
O(1)	8*j*	0.266(1)	0.333	0.754(1)	1	1
O(2)	4*i*	0.266(1)	0	0.754(1)	1	1

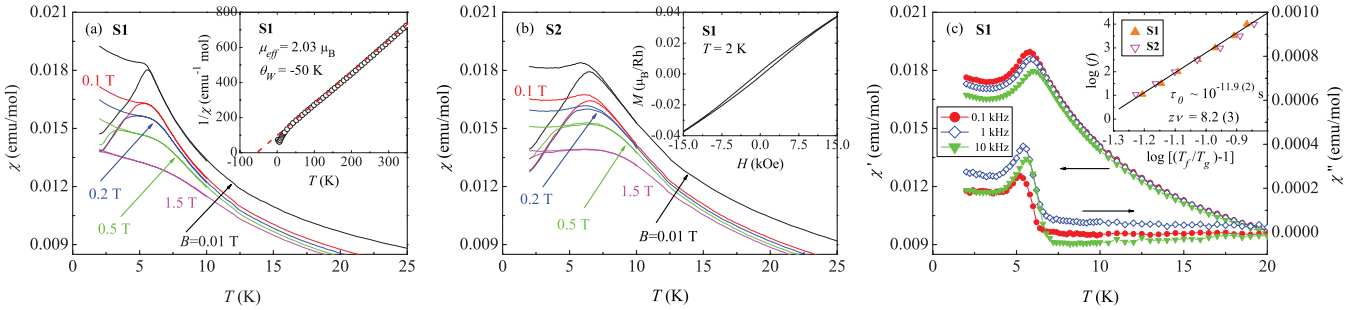

FIG. 3. (Color online) Temperature dependent magnetic susceptibility of Li_2RhO_3. (a), (b) $\chi(T)$ of S1 and S2 measured under various fields, respectively, in both ZFC and FC processes. The inset of (a) displays a Curie-Weiss fit of $1/\chi(T)$ in the high T region, while the inset of (b) shows a hysteretic loop in $M(H)$ below T_g. (c) ac susceptibility measurement of S1. Inset of (c): Scaling plot of $\log(f)$ vs $\log[(T_f/T_g)-1]$ for S1 (solid) and S2 (open), with the best fitted parameters $\tau_0 \sim 10^{-11.9(2)}$ s, $z\nu = 8.2(3)$, $T_{g1} = 5.30$ K, and $T_{g2} = 5.97$ K. The solid line is a guide to the eyes of this fitting.

samples [e.g., the result of S2 is shown in Fig. 3(b)], although the peak position may vary slightly in the range of 5–7 K.

All these phenomena are hard to be understood by a simple AFM or ferromagnetic (FM) transition, but remind us of the spin-glass transition. We therefore performed the ac magnetic susceptibility of Li_2RhO_3, and the results are displayed in Fig. 3(c). Indeed, a peak in the imaginary part of ac susceptibility χ'' is evidently seen, strongly demonstrating the dissipative process. In addition, the real part of ac susceptibility χ' shows a peak at the freezing temperature (T_f), which shifts towards a higher temperature with increasing frequency (f). Such a frequency dependent dissipative process is a fingerprint of a spin-glass transition. The frequency dependence of T_f can be described by the conventional "critical slowing down" of the spin dynamics:[21–23]

$$\tau(T_f) = \tau_0(T_f/T_g - 1)^{-z\nu}, \qquad (1)$$

where $\tau = 1/f$, T_g is the characteristic temperature of the spin-glass transition for $f \to 0$, $z\nu$ is a dynamical exponent, while τ_0 characterizes the intrinsic relaxation time of spin dynamics. We show this agreement by plotting $\log(f)$ vs $\log[(T_f/T_g) - 1]$ in the inset of Fig. 3(c). The results of S1 and S2 can be well scaled into the same curve in this plot, with the parameters of this scaling law $z\nu = 8.2(3)$, $\tau_0 \sim 10^{-11.9(2)}$ s, while the critical temperatures for the two samples are $T_{g1} = 5.30$ K and $T_{g2} = 5.97$ K, respectively. The value of $z\nu$ is in good agreement with the theoretical prediction (7.0–8.0) for an Ising spin-glass system.[24,25] The derived τ_0 is in close approximation to that of a single atomic spin-glass system which usually possesses a τ_0 in the order of 10^{-13} s, implying that the observed spin-glass behavior is likely to arise from the frustrated single Rh^{4+} ions in the honeycomb lattice, rather than from magnetic domains or clusters (for which τ_0 can be as large as 10^{-4} s[26]).

We now turn to the specific heat of Li_2RhO_3, as is shown in Fig. 4. The measurement was carried out on sample S1. An anomaly is clearly seen at around 7 K. Such an anomaly differs from a λ-shaped specific heat jump usually seen in a second order phase transition, indicating the absence of long-range magnetic ordering, and is consistent with the spin-glassy feature.[27] Under magnetic field, this anomaly is suppressed and a Brillouin-like polarization trend is observable. Such an evolution of specific heat under field provides further evidence of the competition between the Zeeman energy and spin-glassy ordering, which is also depicted by the broadened spin-freezing peaks in $\chi(T)$ [Figs. 3(a) and 3(b)]. We should emphasize that no long-range magnetic ordering can be captured down to 0.5 K in Li_2RhO_3 by specific heat measurements. For comparison, the specific heat of its nonmagnetic reference Li_2SnO_3 was also measured. We fit the specific heat of Li_2SnO_3 to the formula $C_{Sn}/T = \gamma_0^{Sn} + \beta^{Sn}T^2$, and the derived Sommerfeld coefficient is $\gamma_0^{Sn} = 0.18\,\mathrm{mJ/(mol\,K^2)}$. Such low γ_0^{Sn} of Li_2SnO_3 signifies its highly insulating electronic property. The slope of this fit results in a Debye temperature $\Theta_D^{Sn} = 418$ K. We calculated the lattice contribution to specific heat in Li_2RhO_3 by correcting C_{Sn} to the molar mass,[28] and the estimated Debye temperature of Li_2RhO_3 is $\Theta_D^{Rh} = 444$ K. The magnetic specific heat in Li_2RhO_3 is obtained by subtracting the lattice contribution from the total specific heat, and the result C_m/T is displayed in the upper inset of Fig. 4. The short-range magnetic ordering

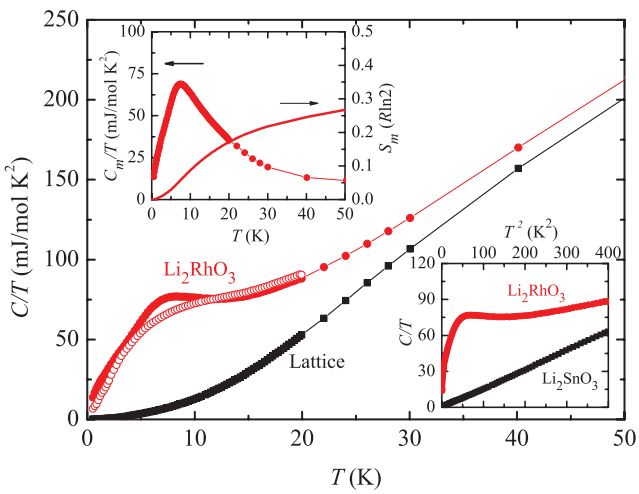

FIG. 4. (Color online) Main frame: Specific heat divided by T of Li_2RhO_3 (red), compared to the lattice contribution (black), which was derived by correcting its nonmagnetic reference Li_2SnO_3. The solid (open) symbols represent data measured under $\mu_0 H = 0$ (9 T). Lower inset: C/T of Li_2RhO_3 and Li_2SnO_3 plot in the T^2 scale. Upper inset: Magnetic contribution to specific heat in Li_2RhO_3; also shown is the magnetic entropy gain S_m as a function of T.

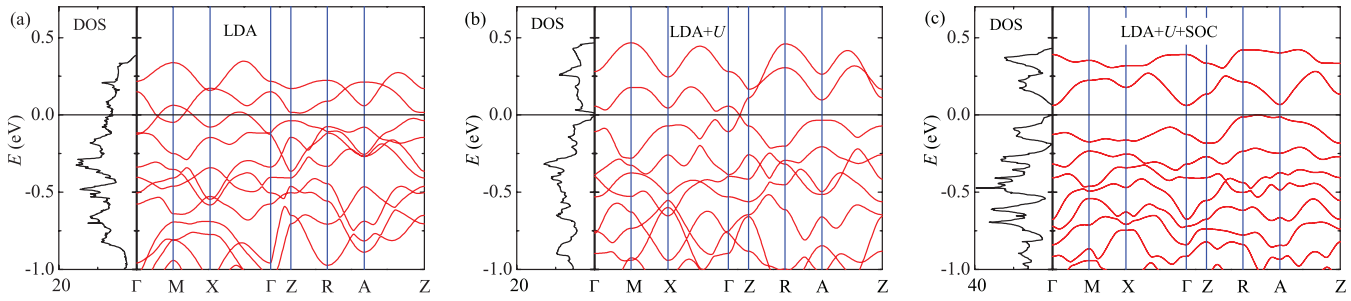

FIG. 5. (Color online) The calculated density of states (DOS) and band structure of Li_2RhO_3, based on (a) LDA, (b) LDA + U (U = 3 eV), and (c) LDA + U + SOC (U = 3 eV). The calculations were performed with stripy-AFM structure.

above T_g is further represented by the noticeable broad tail in C_m/T. We then calculated the magnetic entropy gain $S_m(T)$ by integrating C_m/T over T. We found that S_m reaches only 17% of $R\ln 2$ at 20 K, and keeps increasing even for T up to 50 K while no evident plateau can be seen (see the upper inset of Fig. 4). There are two sources of entropy gain loss. Besides the short-range magnetic ordering mentioned above, more magnetic entropy [$\sim$70% of $R\ln 2$, judging from S_m(50 K)] should be compensated by the residual magnetic entropy stemming from the quantum magnetic randomness that persists even at zero temperature, consistent with the spin-glass scenario.

To well understand these experimental results, we performed a first-principles calculation.[29] For the 4d transition metal element, both electronic correlation and SOC should be taken into account. The calculated density of states (DOS) and band structure are shown in Fig. 5. We started with the local density approximation (LDA), from which we derived a metallic electronic state [Fig. 5(a)] as Rh^{4+} has a half-filled ionic configuration of $4d^5$. The application of Coulomb repulsion U = 3 eV (Ref. 30) greatly reduces the DOS at the Fermi level, however, there are still two bands crossing the Fermi level [Fig. 5(b)] and forming a semimetal-like band structure. We should point out that such a semimetal-like band structure is robust to Coulomb repulsion and will persist even under $U > 4$ eV (data not shown). SOC was then employed, and the combination of U and SOC successfully eliminates the band crossing at the Fermi level and thus opens a gap $\Delta \sim 65$ meV in the DOS spectrum, as shown in Fig. 5(c). This magnitude of the energy gap is close to the thermal activating gap (78 meV) derived experimentally. The calculated SOC splitting is $\sim$10 meV, much smaller than that of Na_2IrO_3,[20] and the orbital- and spin-moment contributions are, respectively,[31] $\langle L\rangle = 0.21\mu_B$/Rh and $\langle S\rangle = 0.19\mu_B$/Rh. We should also point out that merely SOC cannot open a gap at the Fermi level either (data not shown). Therefore, Li_2RhO_3 is suggested to be a relativistic Mott insulator driven by both electronic correlation and SOC.

The calculation also helps us understand the spin-glassy feature of Li_2RhO_3. The study of such a SOC mediated honeycomb lattice turns to the Heisenberg-Kitaev model,[32–36] in which FM ordering, AFM ordering with Néel-, stripy, or zigzag-type ground state, or a spin-liquid state emerges, depending on the particular anisotropic magnetic couplings. In the case of Li_2RhO_3, the calculation based on LDA + U prefers a FM ground state, but is challenged by several other magnetic configurations. When SOC is turned on, the ground state may switch to the stripy- or zigzag-type AFM configuration,[29] and still many other magnetic configurations are comparable in energy. In this situation, perturbations such as disorders or defects (see Table I) are likely to change the magnetic ground state. It is a fact that Li_2RhO_3 embeds in a regime close to the multiphase boundary that results in the spin-glass nature. In addition, according to Choi *et al.*'s result of an inelastic neutron scattering experiment on single crystalline Na_2IrO_3, there is some proportion of the stacking fault of well-ordered honeycomb layers along the c axis,[37,38] which is hardly resolvable by a powder XRD pattern.[9] Such a stacking fault might also appear in Li_2RhO_3 and account for spin-glass ordering. To clarify the magnetism of Li_2RhO_3, single crystals are highly needed. With a moderate strength of electronic correlation and SOC, our result sheds light on the research of the Heisenberg-Kitaev model in realistic materials and calls for more investigations in the future.

To summarize, we systematically studied the electronic and magnetic properties of Li_2RhO_3 on polycrystalline samples. Our experiment confirms that Li_2RhO_3 is a spin-glassy insulator with a narrow gap $\Delta \sim 78$ meV. This picture is supported by a first-principles calculation which verifies the combination of electronic correlation and SOC. The calculation also points to many nearly degenerated magnetic configurations, which possibly illustrates spin-glass behavior. Our result provides a unique case for studies of the Heisenberg-Kitaev model in realistic materials with moderate electronic correlation and SOC.

Y. Luo thanks Hui Xing and Ying Liu for helpful discussions. This work was supported by the National Basic Research Program of China (Grants No. 2011CBA00103, No. 2012CB927404, and No. 2010CB923003), the National Science Foundation of China, and the Fundamental Research Funds for the Central Universities of China.

*zhuan@zju.edu.cn

[1] J. G. Bednorz and K. A. Müller, Z. Phys. B **64**, 189 (1986).

[2] R. von Helmolt, J. Wecker, B. Holzapfel, L. Schultz, and K. Samwer, Phys. Rev. Lett. **71**, 2331 (1993).

[3] Y. Maeno, H. Hashimoto, K. Yoshida, S. Nishizaki, T. Fujita, J. G. Bednorz, and F. Lichtenberg, Nature (London) **372**, 532 (1994).

[4] K. D. Nelson, Z. Q. Mao, Y. Maeno, and Y. Liu, Science **306**, 1151 (2004).

[5]K. Takada, H. Sakurai, E. T. Muromachi, F. Izumi, R. A. Dilanian, and T. Sasaki, Nature (London) **422**, 53 (2003).
[6]R. S. Perry, L. M. Galvin, S. A. Grigera, L. Capogna, A. J. Schofield, A. P. Mackenzie, M. Chiao, S. R. Julian, S. I. Ikeda, S. Nakatsuji, Y. Maeno, and C. Pfleiderer, Phys. Rev. Lett. **86**, 2661 (2001).
[7]D. Yanagishima and Y. Maeno, J. Phys. Soc. Jpn. **70**, 2880 (2001).
[8]A. S. Erickson, S. Misra, G. J. Miller, R. R. Gupta, Z. Schlesinger, W. A. Harrison, J. M. Kim, and I. R. Fisher, Phys. Rev. Lett. **99**, 016404 (2007).
[9]Y. Singh and P. Gegenwart, Phys. Rev. B **82**, 064412 (2010).
[10]B. J. Kim, Hosub Jin, S. J. Moon, J. Y. Kim, B. G. Park, C. S. Leem, J. Yu, T. W. Noh, C. Kim, S. J. Oh, J. H. Park, V. Durairaj, G. Cao, and E. Rotenberg, Phys. Rev. Lett. **101**, 076402 (2008).
[11]R. S. Perry, F. Baumberger, L. Balicas, N. Kikugawa, N. J. C. Ingle, A. Rost, J. F. Mercure, Y. Maeno, Z. X. Shen, and A. P. Mackenzie, New J. Phys. **8**, 175 (2006).
[12]M. Jansen and R. Hoppe, Z. Anorg. Allg. Chem. **397**, 279 (1973).
[13]G. Lang, Z. Anorg. Allg. Chem. **348**, 246 (1966).
[14]V. Todorova and M. Jansen, Z. Anorg. Allg. Chem. **637**, 37 (2011).
[15]H. Kobayashi, R. Kanno, Y. Kawamoto, M. Tabuchi, O. Nakamura, and M. Takano, Solid State Ionics **82**, 25 (1995).
[16]H. Kobayashi, M. Tabuchi, M. Shikano, H. Kageyamaa, and R. Kannob, J. Mater. Chem. **13**, 957 (2003).
[17]M. J. O'Malley, H. Verweij, and P. M. Woodward, J. Solid State Chem. **181**, 1803 (2008).
[18]F. Izumi and K. Momma, Solid State Phenom. **130**, 15 (2007).
[19]P. V. E. McLintock, D. J. Meredith, and J. K. Wigmore, *Matter at Low Temperatures* (Blackie, Glasgow, 1984), p. 82.
[20]R. Comin, G. Levy, B. Ludbrook, Z. H. Zhu, C. N. Veenstra, J. A. Rosen, Yogesh Singh, P. Gegenwart, D. Stricker, J. N. Hancock, D. van der Marel, I. S. Elfimov, and A. Damascelli, Phys. Rev. Lett. **109**, 266406 (2012).
[21]K. Binder and A. P. Young, Phys. Rev. B **29**, 2864 (1984).
[22]J. A. Mydosh, *Spin Glasses: An Experiment Introduction* (Taylor & Francis, London, 1993).
[23]K. Gunnarsson, P. Svedlindh, P. Nordblad, L. Lundgren, H. Aruga, and A. Ito, Phys. Rev. Lett. **61**, 754 (1988).
[24]S. Kirkpatrick and D. Sherrington, Phys. Rev. B **17**, 4384 (1978).
[25]I. A. Campbell, Phys. Rev. B **33**, 3587 (1986).
[26]A. K. Bera and S. M. Yusuf, Phys. Rev. B **86**, 024408 (2012).
[27]K. H. Fischer and J. A. Hertz, *Spin Glasses* (Cambridge University Press, Cambridge, UK, 1991), p. 301.
[28]M. Bouvier, P. Lethuillier, and D. Schmitt, Phys. Rev. B **43**, 13137 (1991).
[29]The calculations were performed with the plane-wave basis projected-augmented wave code VASP, with the Perdew-Burke-Ernzerhof (PBE) flavor of the generalized gradient approximation (GGA) chosen to be the exchange-correlation functional. The total energy cutoff was set to be 540 eV and an $8 \times 5 \times 8\Gamma$-centered K mesh was used. For more details of the calculation, please refer to C. Cao, Y. Luo, Z. Xu, and J. Dai, arXiv:1303.4675.
[30]S. L. Dudarev, G. A. Botton, S. Y. Savrasov, C. J. Humphreys, and A. P. Sutton, Phys. Rev. B **57**, 1505 (1998).
[31]X. Wan, A. M. Turner, A. Vishwanath, and S. Y. Savrasov, Phys. Rev. B **83**, 205101 (2011).
[32]A. Kitaev, Ann. Phys. (NY) **321**, 2 (2006).
[33]J. Chaloupka, G. Jackeli, and G. Khaliullin, Phys. Rev. Lett. **105**, 027204 (2010).
[34]H. C. Jiang, Z. C. Gu, X. L. Qi, and S. Trebst, Phys. Rev. B **83**, 245104 (2011).
[35]X. Liu, T. Berlijn, W. G. Yin, W. Ku, A. Tsvelik, Y. J. Kim, H. Gretarsson, Y. Singh, P. Gegenwart, and J. P. Hill, Phys. Rev. B **83**, 220403(R) (2011).
[36]Y. Singh, S. Manni, J. Reuther, T. Berlijn, R. Thomale, W. Ku, S. Trebst, and P. Gegenwart, Phys. Rev. Lett. **108**, 127203 (2012).
[37]S. K. Choi, R. Coldea, A. N. Kolmogorov, T. Lancaster, I. I. Mazin, S. J. Blundell, P. G. Radaelli, Y. Singh, P. Gegenwart, K. R. Choi, S. W. Cheong, P. J. Baker, C. Stock, and J. Taylor, Phys. Rev. Lett. **108**, 127204 (2012).
[38]F. Ye, S. Chi, H. Cao, B. C. Chakoumakos, J. A. Fernandez-Baca, R. Custelcean, T. F. Qi, O. B. Korneta, and G. Cao, Phys. Rev. B **85**, 180403(R) (2012).